Supplementary information

Exploring new heterobimetallic ferrocenyl derivatives as prospective antitrypanosomal agents

Esteban Rodríguez Arce[a], Eugenia Putzu[a], Michel Lapier[b], Juan Diego Maya[c], Claudio Olea Azar[b], Gustavo A. Echeverría[d], Oscar E. Piro[d], Andrea Medeiros[e,f], Florencia Sardi[e], Marcelo Comini[e], Gastón Risi[g], Isabel Correia,[h] João Costa Pessoa,[h] Lucía Otero[a*], Dinorah Gambino[a*]

[a] Química Inorgánica, Facultad de Química, Universidad de la República, Gral. Flores 2124, 11800 Montevideo, Uruguay.

[b] Departamento de Química Inorgánica y Analítica, Facultad de Ciencias Químicas y Farmacéuticas, Universidad de Chile, Casilla 233, Santiago, Chile.

[c] ICBM, Facultad de Medicina, Universidad de Chile, Av. Independencia 1027, Santiago, Chile.

[d] Departamento de Física, Facultad de Ciencias Exactas, Universidad Nacional de La Plata and Institut IFLP (CONICET, CCT-La Plata), C.C. 67, 1900 La Plata, Argentina.

[e] Group Redox Biology of Trypanosomes, Institut Pasteur de Montevideo, Mataojo 2020, CP 11400, Montevideo, Uruguay

[f] Departamento de Bioquímica, Facultad de Medicina, Universidad de la República, Gral. Flores 2125, 11800 Montevideo, Uruguay.

[g] Worm Biology Lab, Institut Pasteur de Montevideo, Montevideo, Uruguay.

[h] Centro de Química Estrutural, Instituto Superior Técnico, Universidade de Lisboa, 1049-001 Lisboa, Portugal

Table S1. Crystal data and structure refinement results for [PdII(L2)(dppf)](PF6), [PtII(L1)(dppf)](PF6) and isomorphic [MII(L3)(dppf)](PF6) (M = Pd, Pt) compounds.

	$[Pt^{II}(L1)(dppf)](PF_6)$	**$[Pd^{II}(L2)(dppf)](PF_6)$**	**$[Pd^{II}(L3)(dppf)](PF_6)$**	**$[Pt^{II}(L3)(dppf)](PF_6)$**
Empirical formula	$C_{40}H_{33}F_6FeN_4O_3P_3PtS$	$C_{41}H_{35}F_6FeN_4O_3P_3PdS$	$C_{42}H_{37}F_6FeN_4O_3P_3PdS$	$C_{42}H_{37}F_6FeN_4O_3P_3PtS$
Formula weight	1107.61	1032.95	1046.97	1135.66
Temperature (K)	296 (2)	296 (2)	297 (2)	297 (2)
Wavelength (Å)	0.71073			
Crystal system	Monoclinic			
Space group	$P2_1/n$			
Unit cell dimensions				
a (Å)	11.2899 (6)	12.7907 (4)	12.8125 (5)	12.7827 (3)
b (Å)	19.654 (1)	10.2881 (3)	10.3191 (5)	10.3154 (3)
c (Å)	18.494 (1)	32.7377 (8)	32.640 (1)	32.6199 (8)
β (°)	97.665 (5)	98.283 (2)	98.143 (4)	98.323 (3)
Volume ($Å^3$)	4067.0 (4)	4263.1 (3)	4272.0 (3)	4255.9 (2)
Z, calculated density (Mg/m^3)	4, 1.809	4, 1.609	4, 1.628	4, 1.772
Absorption coefficient (mm^{-1})	4.034	0.994	0.993	3.858
F(000)	2176	2080	2112	2240
Crystal size (mm^3)	0.226 x 0.123 x 0.073	0.337 x 0.121 x 0.033	0.026 x 0.104 x 0.206	0.062 x 0.118 x 0.356
ϑ-range for data collection (º)	2.872 to 27.000	3.032 to 27.000	3.203 to 26.999	3.205 to 26.998
Index ranges	-13≤h≤14, -17≤k≤25, -23≤l≤19	-15≤h≤16, -13≤k≤12, -39≤l≤41	-16≤h≤15, -13≤k≤13, -40≤l≤41	-16≤h≤15, -13≤k≤9, -41≤l≤41
Reflections collected	23769	20038	23277	25067

Independent reflections	8783 [R(int) = 0.0771]	9171 [R(int) = 0.0304]	9193 [R(int) = 0.0564]	9179 [R(int) = 0.0593]
Obs. reflections [I>2σ(I)]	5487	7379	6293	7840
Completeness (%)	99.8 (to ϑ=25.242°)	99.8 (to ϑ=25.242°)	99.8 (to ϑ=25.242°)	99.8 (to ϑ=25.242°)
Refinement method	Full-matrix least-squares on F^2			
Data / restraints / parameters	8783/0/532	9171/0/542	9193/0/550	9179/0/550
Goodness-of-fit on F^2	1.029	1.064	1.033	1.138
Final R indices[a] [I>2σ(I)]	R1 = 0.0567, wR2 = 0.1238	R1 = 0.0431, wR2 = 0.0961	R1 = 0.0506, wR2 = 0.0829	R1 = 0.0423, wR2 = 0.0945
R indices (all data)	R1 = 0.1144, wR2 = 0.1598	R1 = 0.0601, wR2 = 0.1053	R1 = 0.0903, wR2 = 0.0977	R1 = 0.0537, wR2 = 0.1000
Larg. diff. peak and hole (e.$Å^{-3}$)	2.088 and -0.928	0.867 and -0.698	0.654 and -0.500	1.330 and -1.537

[a] $R_1=\Sigma||F_o|-|F_c||/\Sigma|F_o|$, $wR_2=[\Sigma w(|F_o|^2-|F_c|^2)^2/\Sigma w(|F_o|^2)^2]^{1/2}$

Viability on T. cruzi (Dm28c clone) trypomastigotes. Vero cells were infected with *T. cruzi* metacyclic trypomastigotes from 15 days old Dm28c clone epimastigote cultures. Subsequently, the trypomastigotes harvested from this culture were used to infect further Vero cell cultures at a multiplicity of infection (MOI) of 10. These trypomastigote-infected Vero cell cultures were incubated at 37 °C in humidified air and 5 % CO_2 for 5 to 7 days. After this time, culture media were collected and centrifuged at 3,000 x g for 5 min. The trypomastigote-containing pellets were resuspended in RPMI media supplemented with 5 % fetal bovine serum and penicillin-streptomycin at a final density of 1×10^7 parasites/mL. 2.10×10^8 trypomastigotes are equivalent to 1 mg of protein or 12 mg of wet weight.[27,28]

IC_{50} values were obtained from dose/response curves:

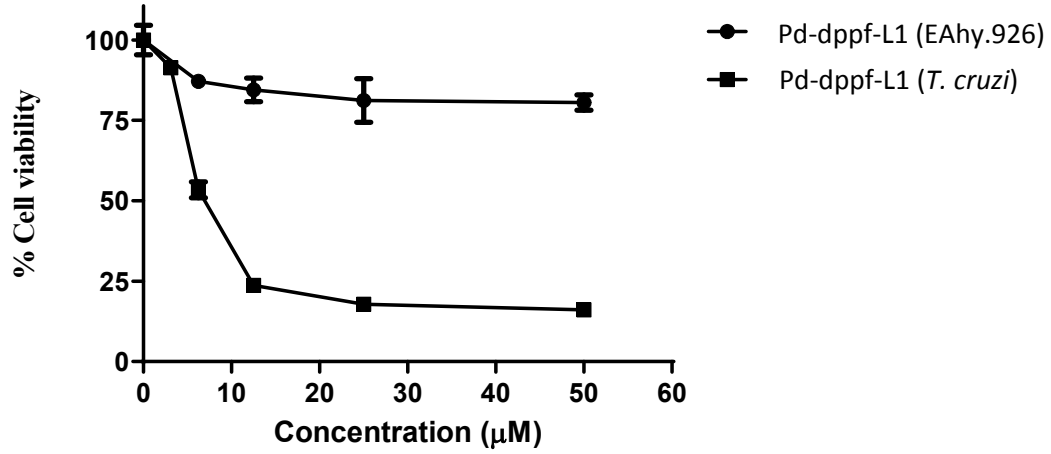

Viability assays for T. brucei. Bloodstream *T. b. brucei* (strain 427) cell line 449 expressing an ectopic copy of the redox biosensor hGrx-roGFP2 was grown in HMI-9 medium complemented with 10 % (v/v) Fetal Bovine Serum Tetracycline-free (FBS; GIBCO) in a humidified incubator with 5 % CO_2 and at 37ºC.[29] Phleomycin (0.2 μg/mL) and hygromycin (5 μg/mL) were added to select for the constitutive expression of the tetracycline repressor protein and for the hGrx-

roGFP2 gene, respectively, whereas the expression of the last was induced by supplementing the medium with 1 µg/mL oxytetracycline for 24 h.

IC_{50} values were obtained from dose/response curves:

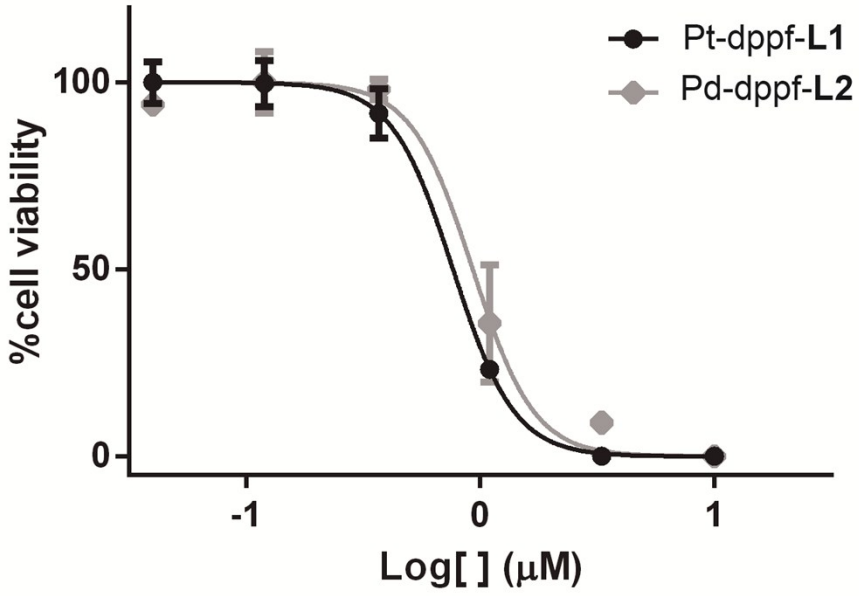

Cytotoxicity on endothelial mammalian cells. The endothelial cell lines EA.hy926 (permanent human cell line derived by fusing human umbilical vein endothelial cells–HUVEC with human lung cells-A549) were maintained in the nutrient medium, Iscove's modified Dulbecco's medium (IMDM) (Sigma–Aldrich) supplemented with 10 % of 25 mM fetal bovine serum, penicillin (100 units/mL), and streptomycin (100 mg/mL). Cells were maintained as a monolayer culture in tissue culture flasks (Thermo Scientific Nunc™) in an incubator at 37 °C in a humidified atmosphere composed of 5 % CO_2.

DNA interaction studies

Fluorescence experiments. Fluorescence emission intensity was corrected for the absorption and emission inner filter effects at the maximum emission wavelength (594 nm) using UV-vis absorption data recorded for each sample according to the following equation.[35]

$$IF_{corr} = IF \times 10^{\left(\frac{Abs_{\lambda_{exc}} + Abs_{\lambda_{em}}}{2}\right)} \quad \text{Eq. (i)}$$

The mechanism involved in the fluorescence quenching process for the compounds was analysed using the Stern-Vomer equation:

$$\frac{IF_0}{IF} = 1 + K_{SV}[Q] \quad \text{Eq. (ii)}$$

where IF_0 and IF are the emission fluorescence intensity of the {DNA-EB} adduct in the absence and in the presence of the complex, K_{SV} is the Stern-Volmer constant, and [Q] correspond to the quencher concentrations (in this case, the complexes).[35]

BSA interaction studies

Fluorescence experiments. The blank´s fluorescence spectrum (containing complex, 2 % DMSO and PBS buffer) was subtracted to each sample´s spectrum, and then they were corrected for the absorption and emission inner filter effects at the maximum emission wavelength (340 nm) using UV-vis absorption data recorded for each sample (Eq. (i)).[35] The mechanism involved in the fluorescence quenching process was analysed using the Stern-Volmer equation (Eq. (ii)).

Moreover, the fluorescence spectroscopic data were used to determine the binding parameters using the Scatchard equation (Eq. (iii)).[38]

$$\log\left[(IF_0 - IF)/IF\right] = logK_{bc} + nlog[Q] \qquad \text{Eq. (iii)}$$

where IF_0 and IF are the fluorescence intensity in the absence and in the presence of the complex, respectively, K_{bc} is the binding constant and n is the number of binding sites.[39,40]

Table S2. Tentative assignment of selected IR absorption bands of the [M(**L**)(dppf)](PF_6) complexes, where M = Pd(II) or Pt(II). Bands of the free thiosemicarbazones H**L1**-H**L4** are included for comparison. Band frequencies are given in cm^{-1}. The code M-dppf-**L** is used for simplicity to identify the [M(**L**)(dppf)](PF_6) compounds.

Compound	**dppf**	**ν(C=N)**	**ν_s (NO_2)**	**ν(N-N)**	**δ (NO_2+furan)**	**ν(P-F), δ(FPF)**
HL1	-	1602	1356	1108	811	-
Pd-dppf-**L1**	1437, 1480, 1098, 698, 493	1605	1353	1098	810	842, 558
Pt-dppf-**L1**	1437, 1480, 1099, 695, 498	1608	1346	1098	810	841, 558
HL2	-	1599	1354	1114	808	-
Pd-dppf-**L2**	1437, 1479, 1096, 696, 494	1591	1350	1097	810	844, 557
Pt-dppf-**L2**	1437, 1479, 1096, 693, 495	1592	1349	1094	812	849, 558
HL3	-	1602	1352	1104	805	-
Pd-dppf-**L3**	1471, 1437, 1097, 694, 500	1591	1345	1098	811	853, 557
Pt-dppf-**L3**	1476, 1437, 1097, 694, 502	1591	1343	1098	812	842, 558
HL4	-	1595	1344	1104	811	-
Pd-dppf-**L4**	1480, 1438, 1099, 692, 492	1598	1348	1097	812	845, 558
Pt-dppf-**L4**	1480, 1438, 1099, 695, 496	1597	1343	1096	812	841, 558

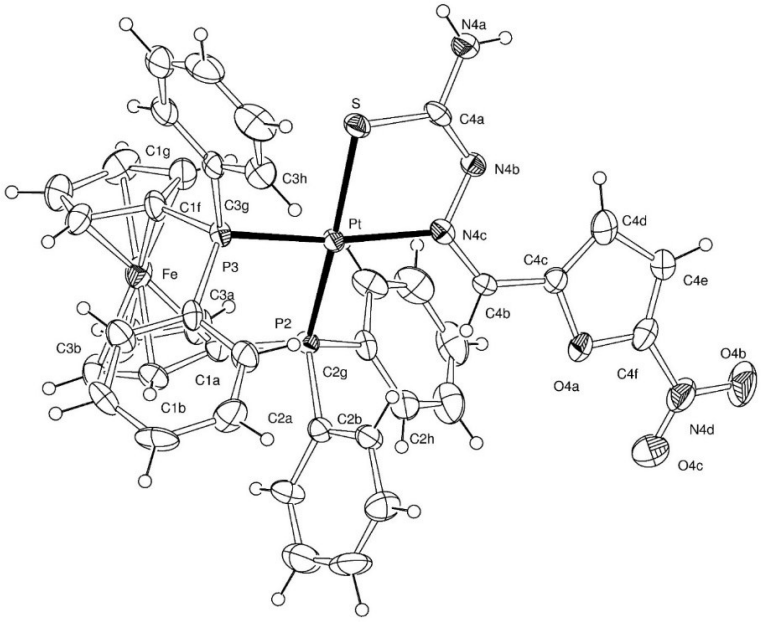

Figure S1. View of [Pt(**L1**)(dppf)](PF_6).

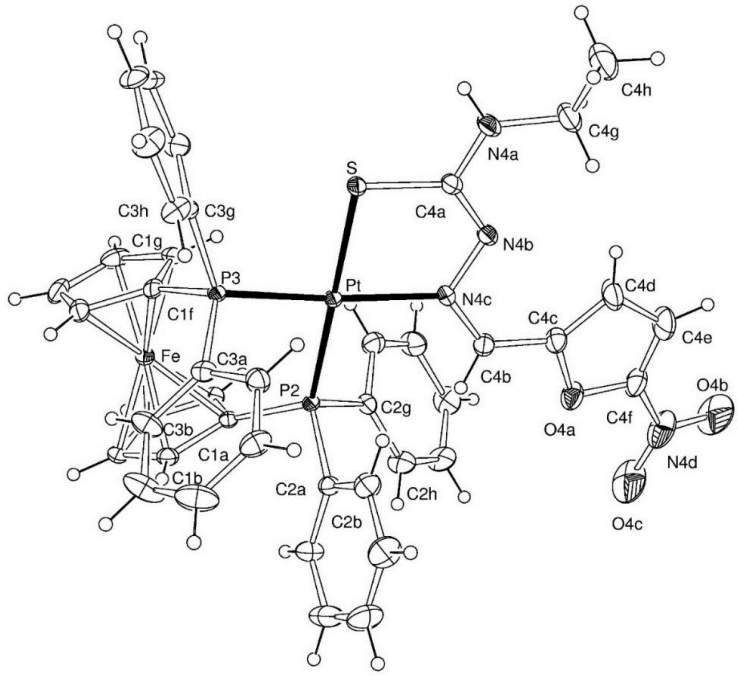

Figure S2. View of [Pt(**L3**)(dppf)](PF_6).

Table S3. ^{1}H NMR chemical shift values (δ, in ppm) of the H**L1**-H**L4** compounds and the corresponding complexes in DMSO-d_6. Compounds are labeled as M-dppf-**L** for simplicity. δ_H (multiplicity, integration)

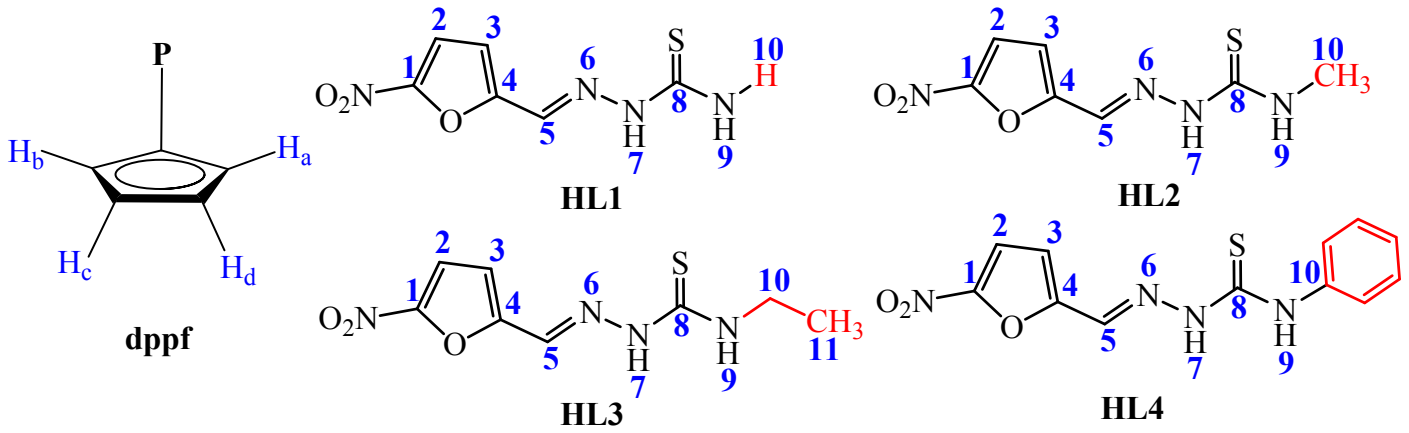

H	HL1	Pd-dppf-L1	Pt-dppf-L1	HL2	Pd-dppf-L2	Pt-dppf-L2	HL3	Pd-dppf-L3	Pt-dppf-L3	HL4	Pd-dppf-L4	Pt-dppf-L4
2	7.80(d,1)	7.91(m,1)[a,b]	7.87(d,1)	7.82(d,1)	7.63(m,1)[a,b]	7.62(m,1)[a,b]	7.83(d,1)	7.63(m,1)[a,b]	7.60(m,1)[a,b]	7.85 (d,1)	7.65(m,1)[a,b]	7.64(m,1)[a,b]
3	7.37(d,1)	7.81(m,1)	7.77(m,1)	7.33 (d,1)	7.40(d,1)	7.47(m,1)[a,b]	7.35(d,1)	7.36(d,1)	7.40(d,1)	7.52 (d,1)	7.34 (m,1)[d]	7.41(m,1)[a,e]
5	7.98 (s,1)	6.61(s,1)	6.93 (s,1)	7.98 (s,1)	6.67(s,1)	7.06(s,1)	7.98(s,1)	6.73(s,1)	7.05 (s,1)	8.09 (s,1)	6.74 (s,1)	7.07 (s,1)
7	11.86(s,1)	-	-	11.93(s,1)	-	-	11.88(s,1)	-	-	12.25(s,1)	-	-
9	8.54 (s,1)	7.76(m,2)[a,b]	8.13 (s, br)	8.58 (s,1)	8.23 (s,1)	8.44 (s,1)	8.61 (s,1)	8.22 (s,1)	8.43 (s,1)	10.20(s,1)	10.19 (s,1)	10.40 (s,1)
10	8.04 (s,1)			3.02 (s,3)	3.83 (s,3)	2.87 (s,3)	2.51 (s,2)	[c]	[c]	-	-	-
11	-	-	-	-	-	-	1.15 (t,3)	1.11 (t,3)	1.11 (t,3)	-	-	-
o	-	-	-	-	-	-	-	-	-	7.54 (d,2)	7.42 (m,2)	7.41 (m,2)[a]
m	-	-	-	-	-	-	-	-	-	7.40 (t,2)	7.34 (m,2)	7.34 (t,2)
p	-	-	-	-	-	-	-	-	-	7.24 (t,1)	7.12 (t,1)	7.14 (t,1)
H_a	-	4.62 (s,2)	3.90 (s,2)	-	4.63 (s,2)	4.64 (s,2)	-	4.64 (s,2)	4.62 (s,2)	-	4.69 (s,4)	4.22 (s,2)
H_b	-	4.77 (s,2)	4.76 (s,4)	-	4.79 (s,2)	4.71 (s,2)	-	4.77 (s,2)	4.75 (s,2)	-	4.76 (s,2)	4.73 (s,2)
H_c	-	4.88 (s,2)		-	4.85 (s,2)	4.75 (s,2)	-	4.81 (s,2)	4.69 (s,2)	-	4.69 (s,4)	4.56 (s,2)
H_d	-	3.86 (s,2)	4.60 (s,2)	-	3.89 (s,2)	3.97 (s,2)	-	3.94 (s,2)	4.00 (s,2)	-	4.16 (s,2)	4.68 (s,2)
PPh_2 dppf	-	7.91 (m,4) 7.76(m,3)[a]	7.95(m,4) 7.75(m,4)	-	7.94 (dd,4) 7.77 (m,4)	7.94 (dd,4) 7.75 (m,4)	-	7.91 (dd,4) 7.76 (m,4)	7.94 (dd,4) 7.75 (m,4)	-	7.93 (m,4) 7.82 (m,4)	7.94 (m,4) 7.81 (m,4)

		7.62 (m,9) 7.46 (m,4)	7.62(m,8) 7.47(m,4)		7.63 (m,8)[a] 7.47 (m,4)	7.62 (m,8)[a] 7.47 (m,4)[a]		7.63 (m,8)[a] 7.47 (m,4)	7.60 (m,8)[a] 7.45 (m,4)		7.65 (m,4)[a] 7.55 (m,8)	7.64 (m,4)[a] 7.54 (m,8)

[a] individual integration obtained from the total integration of the multiplet
[b] overlapped with PPh_2 protons
[c] overlapped with the solvent
[d] overlapped with *meta* protons of the phenyl group
[e] overlapped with *orto* protons of the phenyl group
Multiplicity: s: singlet, d: doublet, t: triplet, m: multiplet

Table S4. Chemical shift values (δ, in ppm) of ^{13}C-NMR of the $[M^{II}(\mathbf{L})(dppf)](PF_6)$ compounds (see numbering in figure in Table S4).

	Pd-dppf-1	**Pt-dppf-L1**	**Pd-dppf-L2**	**Pt-dppf-L2**	**Pd-dppf-L3**	**Pt-dppf-L3**	**Pd-dppf-L4**	**Pt-dppf-L4**
2	135.12	135.09	133.09	133.13	132.82	132.92	132.99	134.34
3	134.93	134.81	122.67	129.10	128.90	128.94	128.66	128.81
5	140.12	141.81	140.98	142.68	143.23	142.72	142.70	142.50
8	174.94	176.44	174.50	177.69	174.54	175.85	173.19	179.08
10	134.20	132.96	33.58	34.07	[a]	[a]	-	-
11	-	-	-	-	14.30	13.59	-	-
***o*-C**	-	-	-	-	-	-	121.45	128.45
***m*-C**	-	-	-	-	-		129.31	129.40
***p*-C**	-	-	-	-	-	-	124.76	128.67
C_a	75.10	76.29	75.09	74.95	74.94	75.22	75.14	73.94
C_b	75.18	75.68	75.70	77.02	77.61	75.60	74.42	77.65
C_c	77.76	77.20	77.99	75.43	77.85	77.11	77.60	75.59
C_d	75.78	74.87	75.80	76.02	76.39	76.30	76.27	77.81
PPh_2	123.08 134.72 129.93 129.00	135.10 134.20 129.32 129.09	134.96 134.22 132.92 129.08	135.22 134.30 129.68 129.13	135.13 134.30 133.05 128.96	135.63 134.93 130.50 128.78	135.38 134.36 132.98 129.76	135.31 134.86 132.36 129.98

[a]: Overlapped with solvent signals

Table S5. Effect of the addition of $[M^{II}(\mathbf{L})(dppf)](PF_6)$ compounds on oxygen uptake by *T. cruzi* epimastigotes (Dm28c strain).

Compound	Increase on oxygen consumption (%)[a]
Pd-dppf-**L1**	23.1
Pt-dppf-**L1**	35.9
Pd-dppf-**L2**	16.5
Pt-dppf- **L2**	22.5
Pd-dppf-**L3**	93.6
Pt-dppf-**L3**	8.2
Pd-dppf-**L4**	24.7
Pt-dppf-**L4**	7.9

[a]: % increase on oxygen consumption after addition of 40 μM of complexes in respect to control (no added compound).

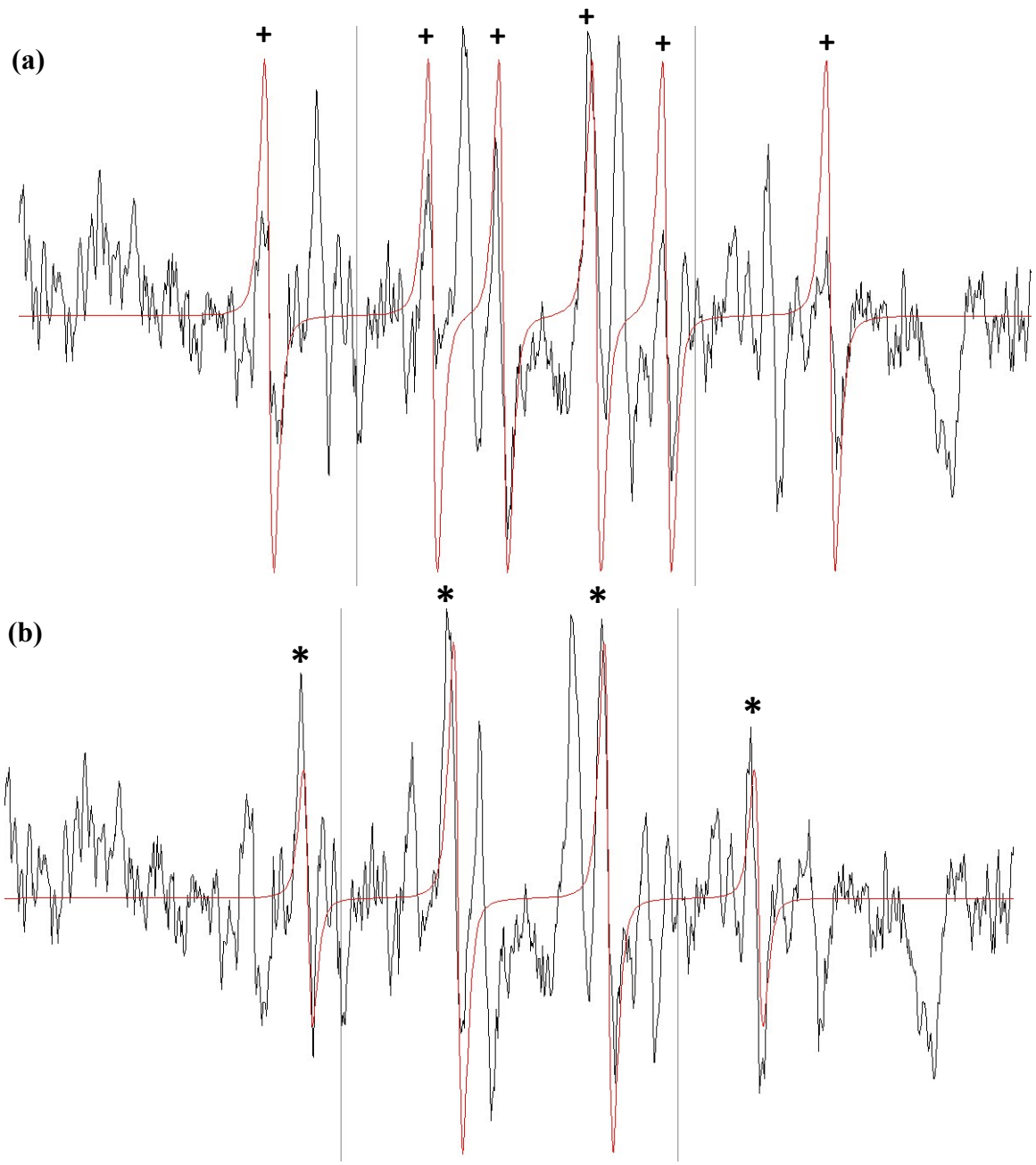

Figure S3. Experimental (black) and simulated (red) ESR spectra obtained after 5 min incubation of [Pd^{II}(**L4**)(dppf)](PF_6) (1 mM) with *T. cruzi* epimastigotes (Dm28c strain, final protein concentration 4-8 mg/mL), NADPH (1 mM) and DMPO (100 mM). (+) characteristic signals of DMPO-nitrocompound spin adduct. (*) characteristic signals of DMPO-OH spin adduct.

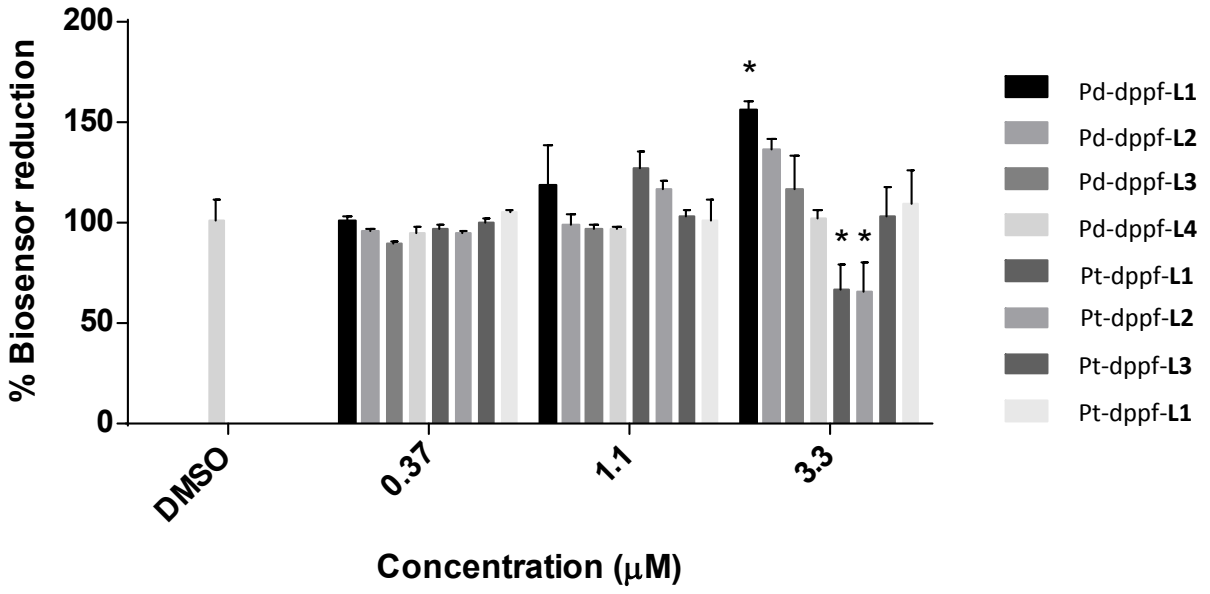

Figure S4. Intracellular redox changes induced by the complexes on bloodstream *T. b. brucei*. Parasites were exposed to 0.37, 1.1 and 3.3 μM of complexes or left untreated (vehicle, 1% v/v DMSO) for 24 h. The values are expressed as percentage (± SD) reduction of the biosensor relative to the control with DMSO (n = 3). Statistical analysis was performed applying One Way ANOVA test followed by Dunnet´s multiple comparisons posttest. * denotes differences with a p value < 0.5 *vs.* DMSO control.

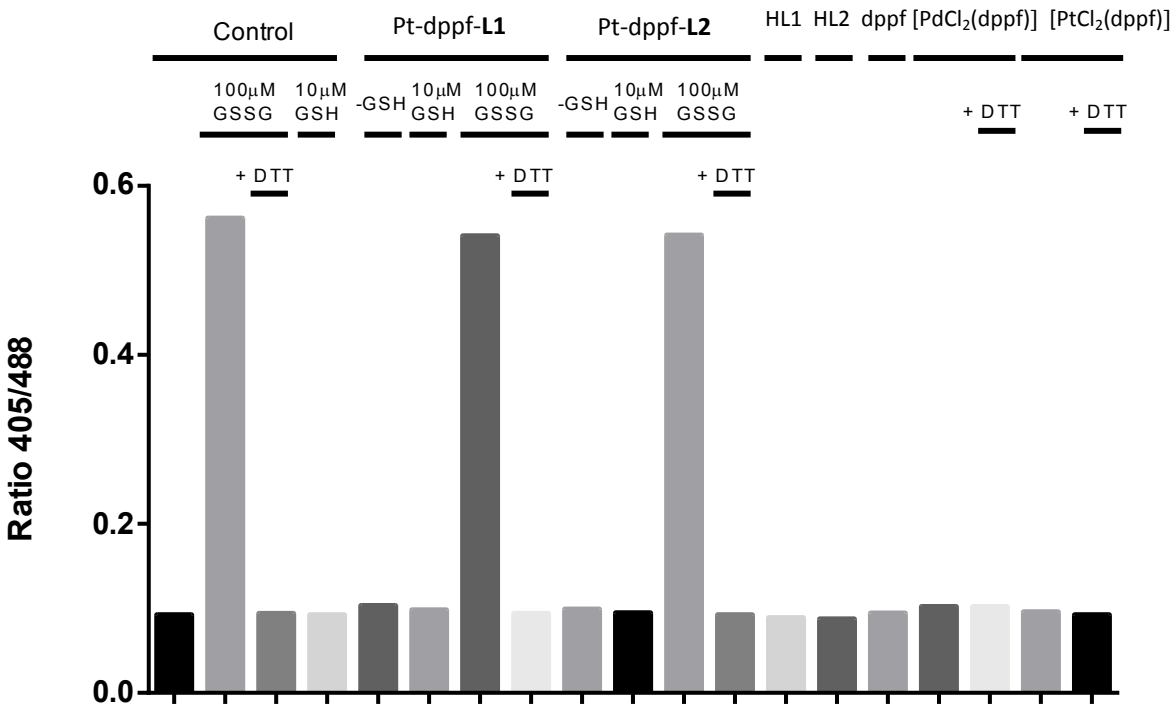

Figure S5. Pt-dppf-**L1** and Pt-dppf-**L2** and their corresponding ligands do not oxidize the redox biosensor or glutathione *in vitro*. The reduced form of the recombinant redox biosensor hGrx-roGFP2 (1 μM) was incubated for 1 h with 10 μM Pt-dppf-**L1** or Pt-dppf-**L2** or their corresponding molecular components (**L1**, **L2**, dppf, [MCl_2(dppf)]) in the absence (-GSH) or presence of 10 μM GSH (only tested for Pt-dppf-**L1** and Pt-dppf-**L2** to determine oxidation of the low molecular weight thiol). The correct response of the redox biosensor (1 μM) was assayed by adding 100 μM GSSG for 1 h followed by treatment with 2 mM DTT for 30 min, in the absence (Control) or presence of 10 μM Pt-dppf-**L1** or Pt-dppf-**L2**. Fluorescence emission at 510 nm was measured upon excitation at 405 nm and 488 nm, and the corresponding 405/488 ratio is plotted. A potential interference of the complexes with the response of the biosensor was ruled out based on the capability of Grx-roGFP2 co-incubated with Pt-dppf-**L1** or Pt-dppf-**L2** to undergo full oxidation by GSSG (100 μM, 1 h) and further reduction by DTT (2 mM, 30 min). On the light of a potential

degradation or disassembly of the compounds at intracellular level, similar assays performed with the different moieties/ligands (10 μM) of both compounds confirmed that none of them induced biosensor oxidation (1 μM) after 1 h incubation.

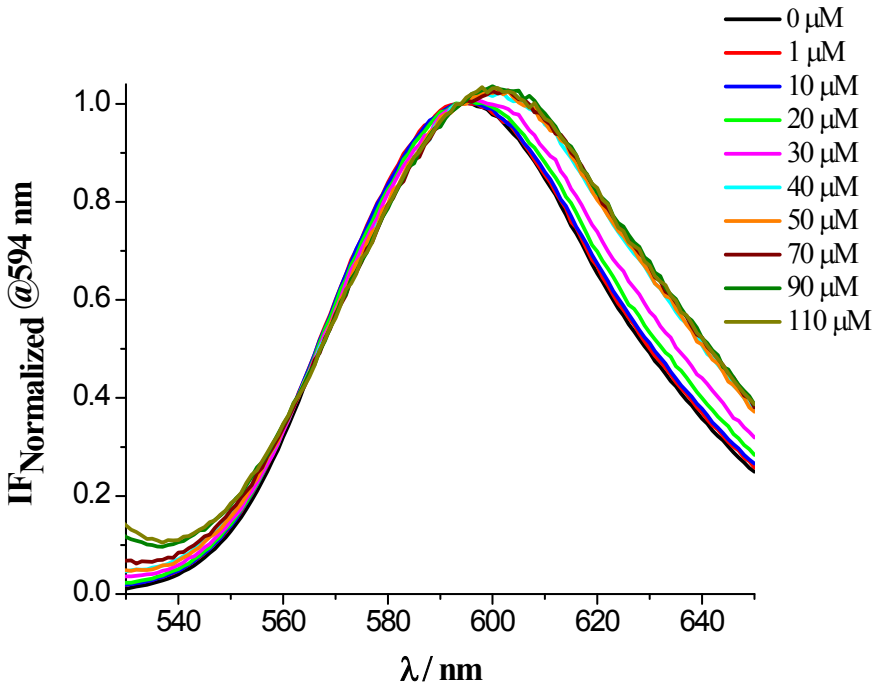

Figure S6. Fluorescence intensity normalized at $\lambda_{em.}$ = 594 nm of the adduct {DNA-EB} at increasing concentrations of the complex [Pd^{II}(**L1**)(dppf)](PF_6).

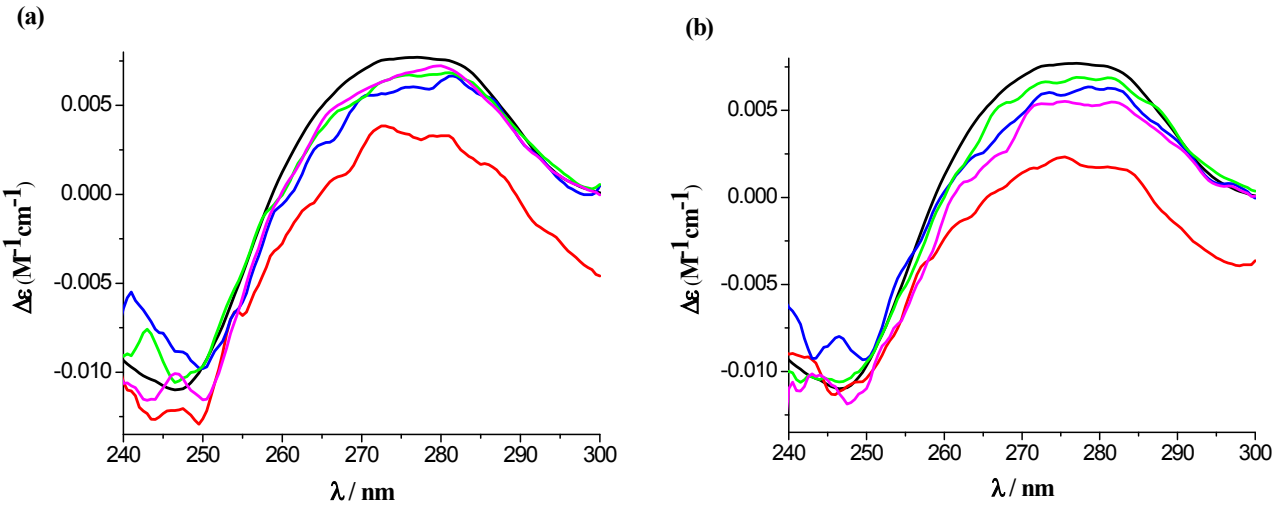

Figure S7. Circular dichroism spectra of CT-DNA (50-60 μM·nucleotide^{-1}) in the absence and presence of (a) palladium and (b) platinum complexes. The Δε values are based on the concentration of DNA. The spectra were measured at zero time using molar ratios DNA/complex of 1:0.5. Black: DNA alone, red: DNA/L1 complexes, blue: DNA/L2 complexes, green: DNA/L3 complexes, violet: DNA/L4 complexes. Optical path quartz cells of 1 cm were used; due to the presence of small amounts of DMSO, the CD spectra measured in the range 240-250 nm are very noisy and the Δε values are only approximate.

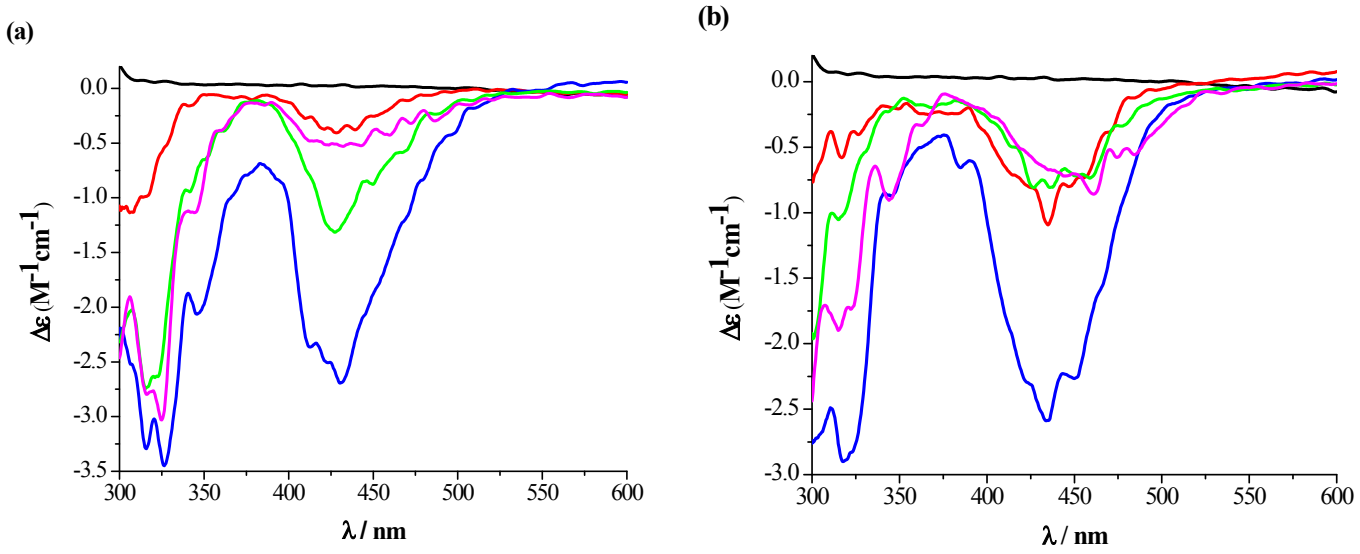

Figure S8. Circular dichroism spectra of CT-DNA (200 μM·nucleotide^{-1}) in the absence and presence of (a) palladium and (b) platinum complexes. The spectra were measured at time zero using molar ratios DNA:complex of 1:0.5. Black: DNA alone, red: DNA/L1 complexes, blue: DNA/L2 complexes, green: DNA/L3 complexes, violet: DNA/L4 complexes. Quartz cells with optical path of 2 cm were used.

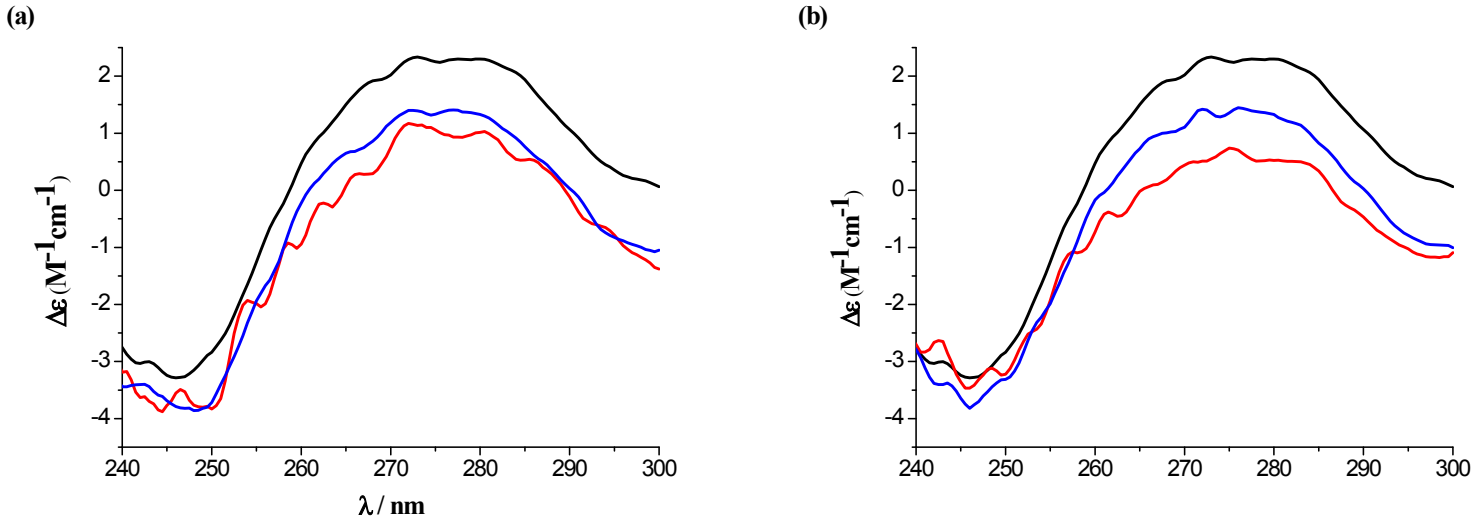

Figure S9. Circular dichroism spectra (1 cm optical path) of CT-DNA (50-60 μM·nucleotide^{-1}) in the absence and presence of (a) [Pd^{II}(**L1**)(dppf)](PF$_6$) and (b) [Pt^{II}(**L1**)(dppf)](PF$_6$) complex. The spectra were measured at time "zero" using different molar ratios of DNA/complex. Black: DNA alone, red: 1:0.5, blue: 1:0.25.

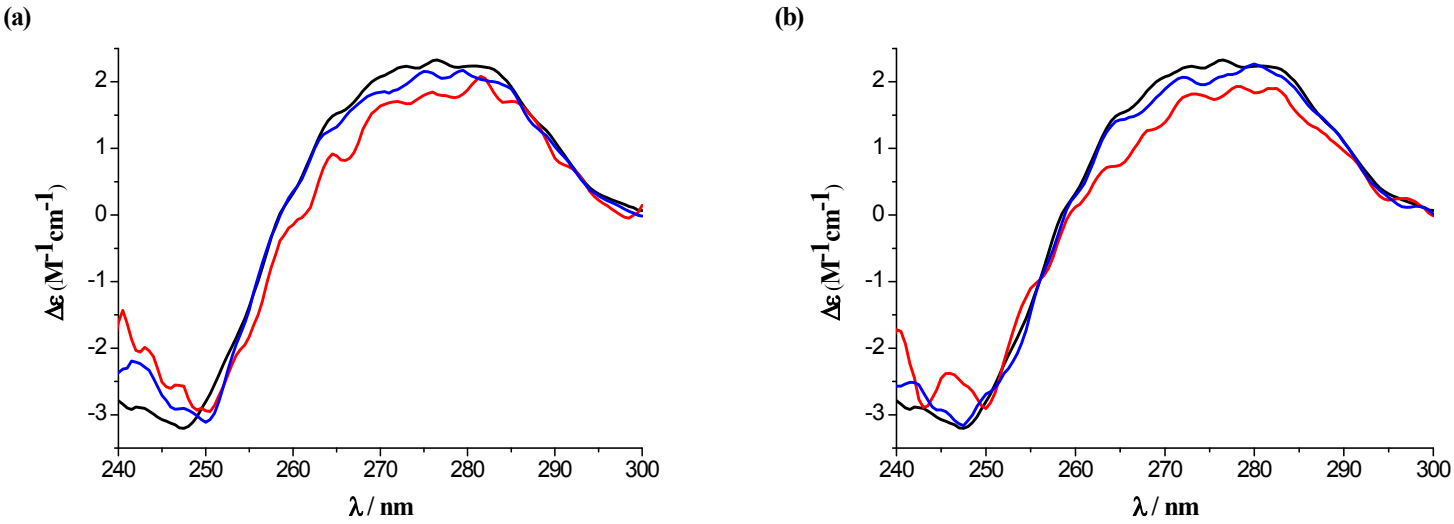

Figure S10. Circular dichroism spectra (1 cm optical path) of CT-DNA (50-60 μM·nucleotide^{-1}) in the absence and presence of (a) [Pd^{II}(**L2**)(dppf)](PF_6) and (b) [Pt^{II}(**L2**)(dppf)](PF_6) complex. The spectra were measured at time zero using different molar ratios of DNA/complex. Black: DNA alone, red: 1:0.5, blue: 1:0.25.

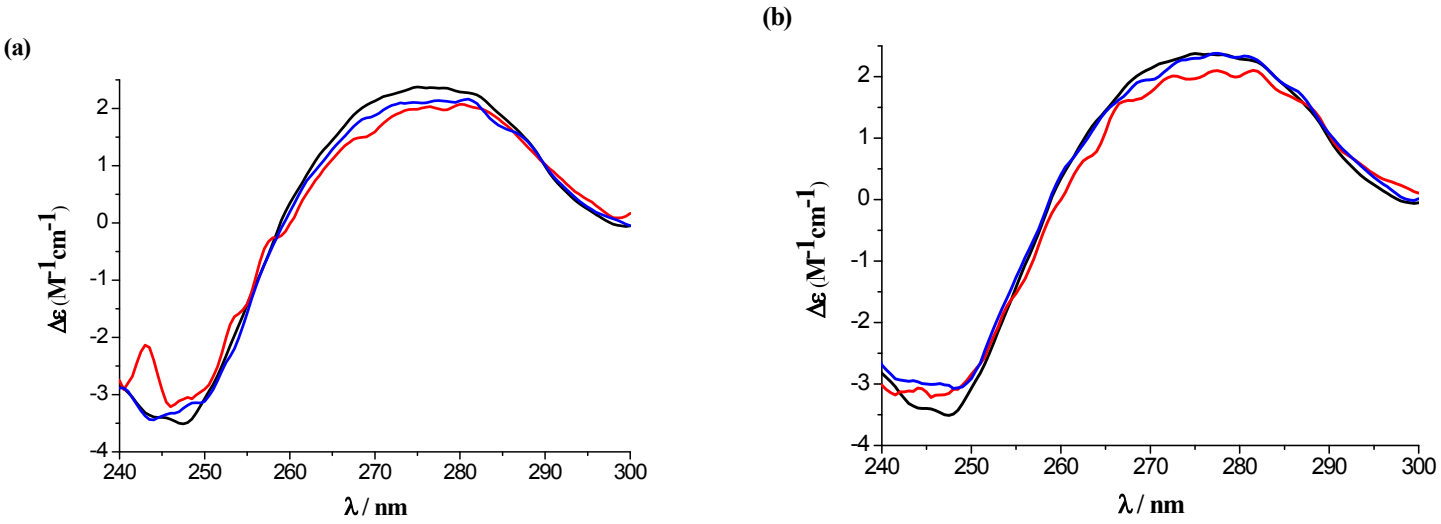

Figure S11. Circular dichroism spectra (1 cm optical path) of CT-DNA (50-60 μM·nucleotide^{-1}) in the absence and presence of (a) [Pd^{II}(**L3**)(dppf)](PF$_6$) and (b) [Pt^{II}(**L3**)(dppf)](PF$_6$) complex. The spectra were measured at time zero using different molar ratios of DNA/complex. Black: DNA alone, red: 1:0.5, blue: 1:0.25.

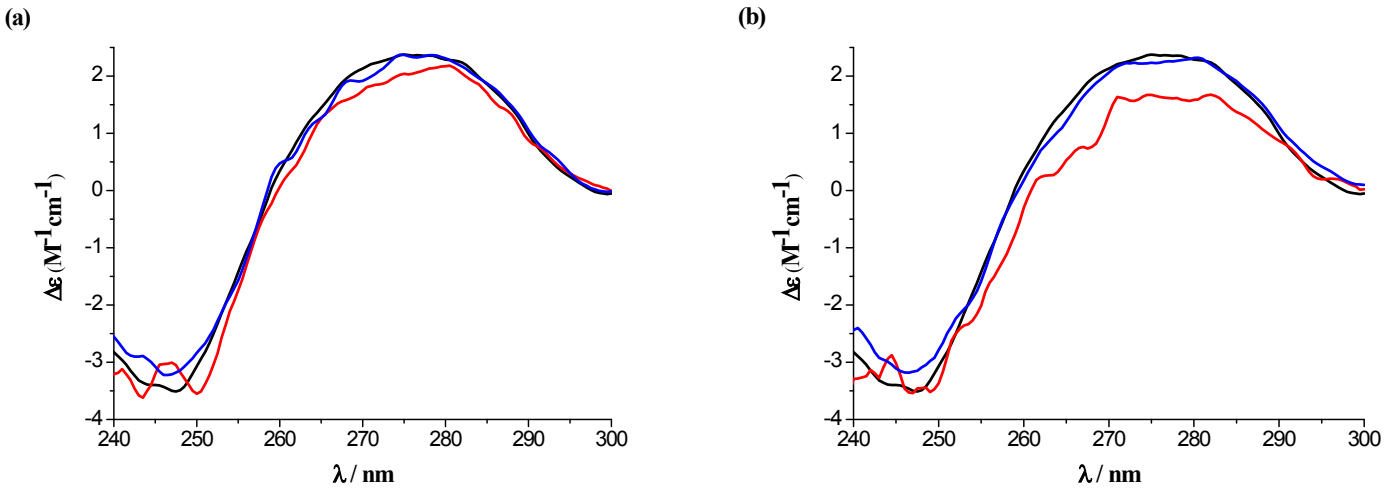

Figure S12. Circular dichroism spectra (1 cm optical path) of CT-DNA (50-60 μM·nucleotide^{-1}) in the absence and presence of (a) [Pd^{II}(**L4**)(dppf)](PF$_6$) and (b) [Pt^{II}(**L4**)(dppf)](PF$_6$) complex. The spectra were measured at time zero using different molar ratios of DNA/complex. Black: DNA alone, red: 1:0.5, blue: 1:0.25.

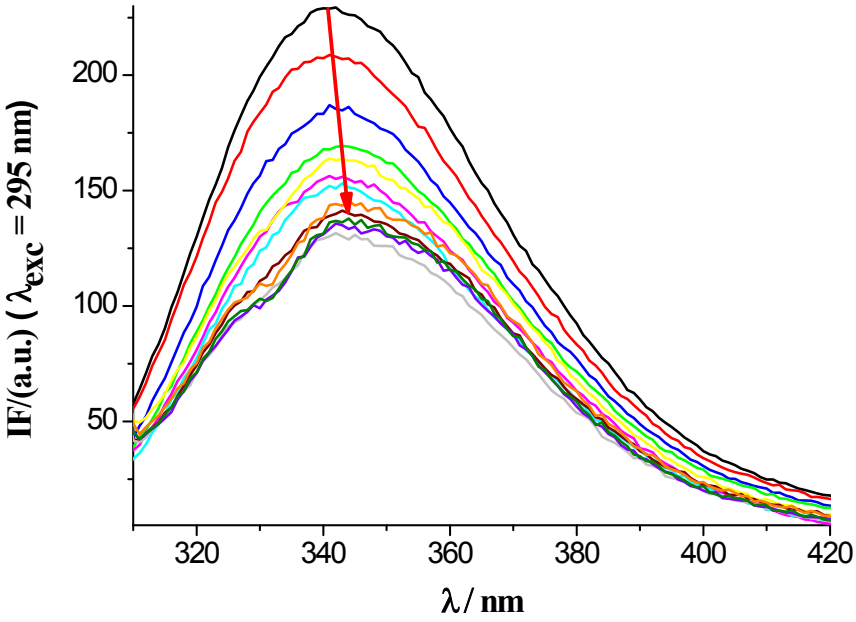

Figure S13. Fluorescence emission spectra of BSA in the absence (black) and in the presence of increasing concentrations of [Pd^{II}(**L3**)(dppf)](PF_6) in 2 % DMSO/10 mM PBS buffer pH 7.4 (C_{BSA} = 1 μM, $C_{complex}$ = 0 - 20 μM, samples prepared individually and incubated for 24 h at 37 °C).

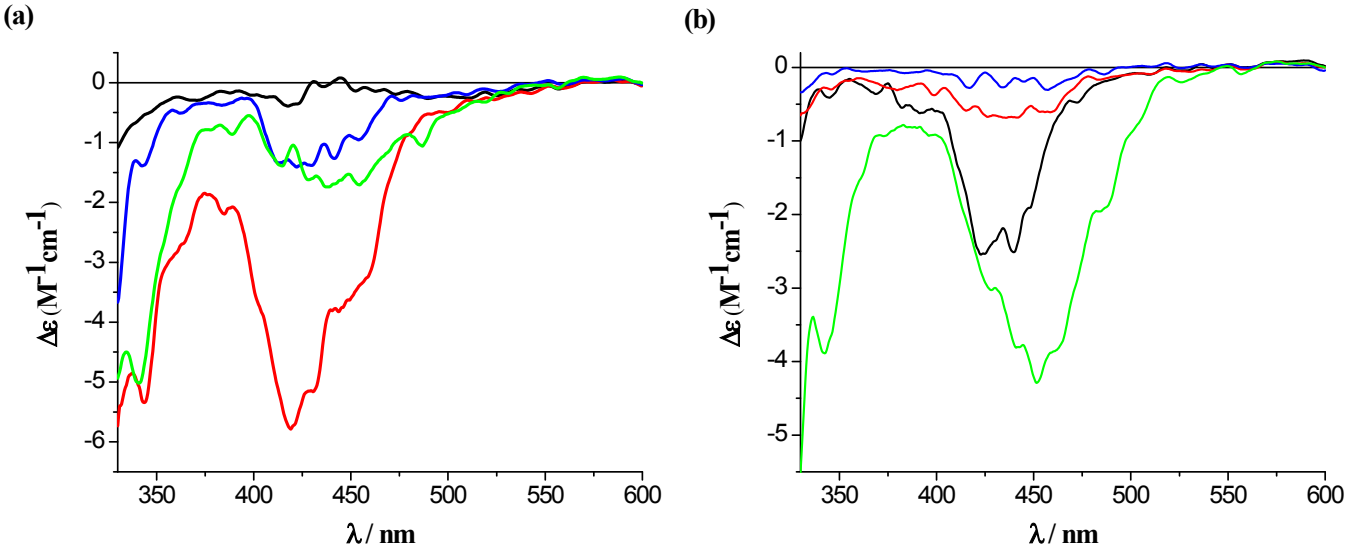

Figure S14. Circular dichroism spectra of solutions containing BSA (100 μM) upon additions of (a) palladium and (b) platinum complexes. The spectra were measured at time zero at 35°C using a molar ratio BSA:complex of 1:1. Black: BSA/L1 complexes, red: BSA/L2 complexes, blue: BSA/L3 complexes, green: BSA/L4 complexes. A quartz cell of 2 cm optical path was used.